Investigation of surface energy, wettability and zeta potential of titanium dioxide/graphene oxide membranes

Pedersen, Morten L. K.; Jensen, Thomas R.; Kucheryavskiy, Sergey V.; Simonsen, Morten E.

Published in:
Journal of Photochemistry and Photobiology A: Chemistry

DOI (link to publication from Publisher):
10.1016/j.jphotochem.2018.07.045

Publication date:
2018

Document Version
Accepted author manuscript, peer reviewed version

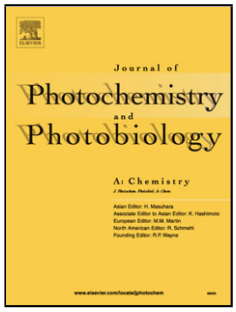

Title: Investigation of surface energy, wettability and zeta potential of titanium dioxide/graphene oxide membranes

Authors: Morten L.K. Pedersen, Thomas R. Jensen, Sergey V. Kucheryavskiy, Morten E. Simonsen

PII: S1010-6030(17)31687-8
DOI: https://doi.org/10.1016/j.jphotochem.2018.07.045
Reference: JPC 11411

To appear in: *Journal of Photochemistry and Photobiology A: Chemistry*

Received date: 15-11-2017
Revised date: 30-7-2018
Accepted date: 30-7-2018

Please cite this article as: Pedersen MLK, Jensen TR, Kucheryavskiy SV, Simonsen ME, Investigation of surface energy, wettability and zeta potential of titanium dioxide/graphene oxide membranes, *Journal of Photochemistry and amp; Photobiology, A: Chemistry* (2018), https://doi.org/10.1016/j.jphotochem.2018.07.045

Investigation of surface energy, wettability and zeta potential of Titanium dioxide/graphene oxide membranes

Morten L. K. Pedersen, Thomas R. Jensen, Sergey V. Kucheryavskiy, Morten E. Simonsen*

Department of Chemistry and Bioscience, Aalborg University, Niels Bohrs Vej 8, 6700, Esbjerg, Denmark

Graphical abstract

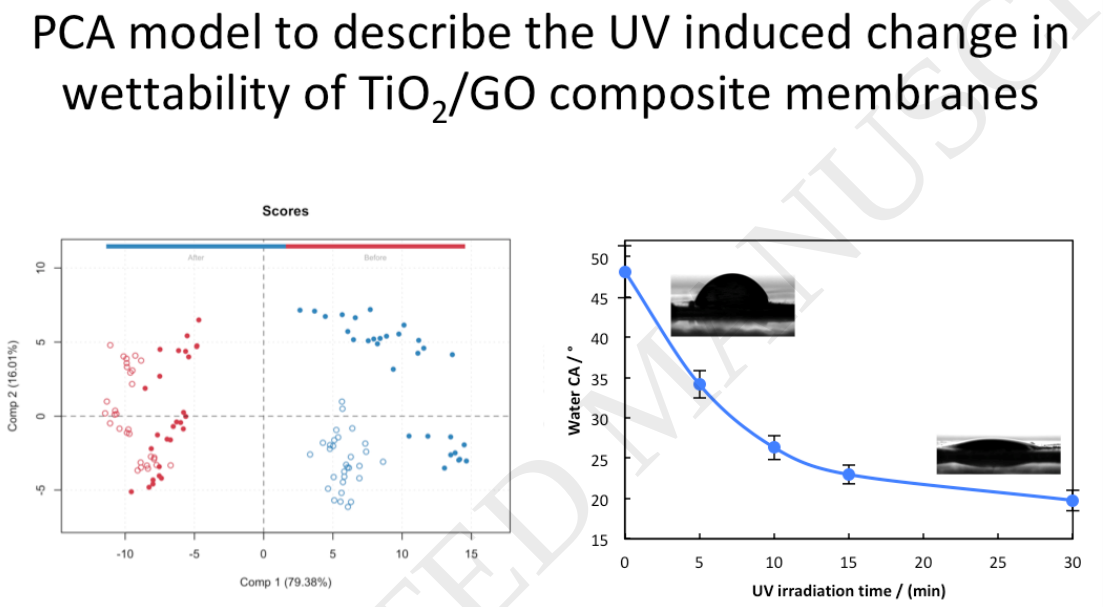

Highlights

- The wettability of pure GO and TiO_2/GO composite membranes are dependent on thermal reduction temperature
- UV activation increases the surface energy and hydrophilicity of the TiO_2/GO membranes
- Principal component analysis of FTIR data was used to generate a model for the change in surface functional group on the TiO_2/GO membranes.
- The zeta potential of the TiO_2/GO membrane surface decreases significantly after UV activation enhancing the electrostatic repulsion of negatively charged fouling components
- The zeta potential of the individual TiO_2/GO membranes is constant in the pH interval 4-9

ABSTRACT: This research aims to study the wettability and zeta potential of photoactive TiO_2/GO composite membranes. Full factorial design was utilized for the investigation of the influence of TiO_2 content, reduction temperature and UV activation on the surface energy and zeta-potential of TiO_2/GO composite membranes. Multivariate data analysis of FTIR data was used to correlate the changes in wettability and zeta-potential after UV irradiation to changes in surface functional groups of the TiO_2/GO membranes.

The hydrophilic properties of pure GO (D) and TiO_2/GO composite membranes (A, B, and C) is highly dependent on reduction temperature; membranes reduced at 140 °C have significantly higher surface energy than membranes reduced at 160 °C. Principal component analysis (PCA) of Fourier transformation infrared spectroscopy (FT-IR) data, thermogravimetry analysis (TGA) and differential scanning calorimetry (DSC) analysis shows that the change in surface energy was a result of loss of carboxylic acid and hydroxyl groups when reduced at 160 °C. The largest change in surface energy was observed after UV activation of the TiO_2/GO membranes. From the PCA model the increase in surface energy is caused by an increase in OH groups on the TiO_2 after activation of the TiO_2/GO membrane.

Moreover higher TiO_2 content was found to significantly increase the surface energy of the membranes. TiO_2/GO membranes with higher TiO_2 contents showed faster hydrophilic conversion rates. In addition the Zeta potential of the membranes changes significantly resulting in more negative zeta potentials after UV activation which enhances the electrostatic repulsion of negatively charged fouling components. The zeta potential of the individual TiO_2/GO membranes was found to be almost constant in the pH interval 4-9.

Keywords

Graphene oxide membrane, TiO_2, Zeta potential, Hydrophilicity, Multi variate data analysis

1. Introduction

In recent years ground water, surface waters and wastewater has been shown to contain an increasing number of contaminants of emerging concern (CEC) like pesticides, pharmaceuticals and hormones. Despite these contaminants are present at low concentrations (ng/L to μg/L) the impact on the ecosystems, human health and availability of clean drinking water is significant [1,2]. Membrane filtration technology has been identified as a key method for removal of CECs in drinking water [2,3]. A major limitation of membrane usage is the fouling phenomena, where the permeate being filtered causes buildup of particles on the membrane surface or in the pores, resulting in a lower flux. Fouling is defined as either reversible or irreversible; reversible fouling can be removed by backwashing, while irreversible fouling can only be removed by chemical cleaning. Backwashing is efficient only for large particles, and chemical cleaning increases running costs significantly and changes the surface properties of membranes [4]. The extent of fouling depends on the electrostatic interaction between the membrane surface and the fouling agent but also the hydrophilicity [5-11]. As many of the often-encountered fouling agents are hydrophobic applying a membrane having a hydrophilic surface can decrease the fouling problem. In this case a water film will cover the membrane surface and provide a steric or energetic barrier against adhesion of fouling components [5, 6]. For charged fouling components electrostatic repulsion between the membrane surface and the components is essential to prevent fouling. [10-11] The electrostatic interactions can be determined by measuring the zeta potential of the membrane surface [10-11].

In the quest for development of more cost effective and efficient membranes, graphene oxide (GO) has in recent years attracted much attention [12, 13]. GO membranes have been found to have excellent selectivity towards water [14] and higher water permeability compared to current commercial reverse osmosis or nano-filtration membranes [14-16]. In addition functionalization of GO by incorporation of photocatalytic active TiO_2 particles to obtain anti-fouling and self-cleaning properties has been investigated [17-20]. TiO_2 in anatase form has long been known to be photocatalytically active, with numerous

studies showing its ability to generate hydroxyl radicals and produce superhydrophilic surfaces upon UV irradiation [21-26]. The formation of hydroxyl radicals allows for breakdown of organic matter on the membrane surface, while the increase in hydrophilicity reduce fouling and improve water flux. The addition of TiO_2 particles has shown promising results in regard to increased flux and anti-fouling properties [17-20]. Other investigations have reported UV light induced reduction of GO both by UV alone [27] and in combination with electron donors (ED) N,N-dimethylformamide [28], phenylbis(2,4,6-trimethylbenzoyl) phosphine oxide [29] or metal oxides ZnO [30] or TiO_2 [31, 32]. In the case of TiO_2 it has been found that carbon atoms with hydroxyl or ether groups are reduced to aromatic carbon while carbonyl and carboxyl groups remain unchanged. This UV induced change in surface functional groups of the GO will influence the wettability and zeta –potential of the TiO_2/GO composite membranes. To the best of our knowledge a detailed study of change in wettability and zeta-potential has not been preformed.

In this study full factorial design was used in the investigation the influence of TiO_2 content, reduction temperature and UV activation on the wettability (surface energy) and zeta-potential of TiO_2/GO composite membranes. This study aims to correlate the changes in wettability and zeta-potential after UV irradiation to changes in surface functional groups of the TiO_2/GO membranes applying multi variate data analysis of FTIR data. In order to study the IR spectral variation before and after UV activation of the TiO_2/GO membranes principal component analysis (PCA) was carried out.

In addition the TiO_2/GO composite membranes were characterized using differential scanning calorimetry (DSC), thermogravimetry analysis (TGA) and X-ray diffraction (XRD).

2. Materials and Methods

2.1. Materials

Graphite powder was obtained from Graphit Kropfmühl GmbH. H_2SO_4 (98%), H_3PO_4 (85%), $KMnO_4$ (99%), H_2O_2 (30%), $NaNO_3$, 1M HCl, titanium-(IV)-isopropoxide (TTIP), glacial acetic acid, 0.1 M HNO_3 were obtained from sigma-aldrich.

2.2 Preparation of GO

The GO synthesizes was based on Tours method [33]. Concentrated H_2SO_4/H_3PO_4 (360:40 mL) was added to a 1000 mL volumetric flask containing graphite powder (3 g) and $KMnO_4$ (18 g), producing a slightly exothermic reaction. The solution was heated to 50°C and stirred for 12 hours. Afterwards, the solution was cooled to room temperature in an ice bath, and 400 mL of water was slowly added to the reaction, always keeping the temperature below 60°C. The synthesis was terminated using 3 mL H_2O_2 (30 %). In order to speed up precipitation, the solution is divided evenly into two beakers and deionized water is added. When the GO had precipitated, the solution was decanted. The remaining solution was rinsed with 1 M HCl and deionized water several times under centrifugation. After centrifugation a stock solution was prepared containing 2.1 w/w % of GO.

2.3. Preparation of TiO_2/GO membranes

The TiO_2 particles were obtained using a microwave assisted sol-gel process, which produces nano-sized TiO_2 (anatase) particles [25, 26]. The synthesis resulted in a suspension of anatase TiO_2 nano-particles (3.6 w/w%). The TiO_2 particles were dispersed using ultrasound (Sonics vibra cell model CV33) before use in the preparation of the TiO_2/GO membranes.

A Full factorial design was applied to investigate the influence of TiO_2 content (4 levels), reduction temperature (2 levels) and UV activation (2 levels) on the wettability of the GO composite membranes. The TiO_2/GO membranes were prepared by mixing 10 g of GO stock solution with the TiO_2 suspension. 4 TiO_2/GO membrane compositions were obtained by varying the TiO_2/GO mixing ratio of the stock

solutions; A: 1:15 (13.4 w/w% TiO_2), B: 1:20 (10.1 w/w% TiO_2), C: 1:30 (6.7 w/w% TiO_2), and D: 0:100 (0 w/w% TiO_2). The percentage ratio between Ti/C in TiO_2/GO composite membranes was verified by SEM-EDX. Homogenization of the TiO_2/GO mixture was achieved using ultrasonication (1 min) and the resulting mixtures were cast into a petri dish (inner diameter 8.7 cm) and dried at room temperature in order to obtain the membrane.

The reduction temperature of the TiO_2/GO membranes were selected to be 140 and 160 °C which both were found to produce stable yet hydrophilic membranes. The TiO_2/GO membranes were reduced at 140 and 160 °C for 1 hour with a heating rate of 5 °C/min under nitrogen atmosphere in a cylindrical Carbolite furnace. In order to avoid damaging the membrane by explosive heating caused by mass transfer limitations [8] the membranes reduced at 160 °C was heated to 140 °C, which was kept for 5 minutes before ramping up to 160 °C at a heating rate of 2.5 °C/min.

The UV activation of the TiO_2/GO membranes was carried out using UVC irradiation (30 min, 254 nm, 2mW/cm^2) level 1 and no irradiation level 0. The experimental design is summarized in table 1.

Table 1. Experimental design with 3 factors: TiO_2 content (4 levels), reduction temperature (2 levels) and UV activation (2 levels).

Sample	TiO_2 content	Reduction Temp.	UV
A TiO_2/GO 140	A	140	0
B TiO_2/GO 140	B	140	0
C TiO_2/GO 140	C	140	0
D GO140	D	140	0
A TiO_2/GO 160	A	160	0
B TiO_2/GO 160	B	160	0
C TiO_2/GO 160	C	160	0
D GO160	D	160	0
A TiO_2/GO 140 UV	A	140	1
B TiO_2/GO 140 UV	B	140	1
C TiO_2/GO 140 UV	C	140	1
D GO140 UV	D	140	1
A TiO_2/GO 160 UV	A	160	1
B TiO_2/GO 160 UV	B	160	1
C TiO_2/GO 160 UV	C	160	1
D GO160 UV	D	160	1

2.4. Membrane characterization

2.4.2 DSC & TGA

The thermal reduction of the GO membranes was investigated using differential scanning calorimetry (DSC) Mettler Toledo DSC822e and thermogravimetry (TGA) Mettler Toledo TGA/SDTA851e. In the DSC experiment the samples were heated to 300°C with a heating rate of 10 °C/min in a nitrogen atmosphere. The sample (3-4 mg) was placed in an aluminum crucible before insertion in the instrument. In the TG analysis the samples were heated to 300°C with a heating rate of 10 °C/min in a nitrogen atmosphere. Small amounts of sample (4 mg) were used to avoid explosion (see section 2.3) during reduction.

2.4.3 X-ray diffraction

X-ray diffraction (XRD) analysis was carried out using a Philips Panalytical X'Pert X-ray diffractometer with a cobalt source running at 45 kV, 20 mA. The distance between layers in the membrane is calculated using Bragg's law:

$$d = \frac{n\lambda}{2 \cdot sin\theta}$$

Where n is the first peak (value 1), λ is the wavelength (0.1789 nm), and θ is the angle of the peak in radians, corresponding to the highest count. The thickness of the stacking layers is calculated using the Scherrer equation:

$$D = \frac{K\lambda}{\beta \cdot cos\theta}$$

Where D is the thickness of the layers, K is the warren shape constant (0,9), λ is the wavelength (0,1789 nm), β is the full width at half maximum (FWHM), θ is the angle [34].

2.4.1 FTIR and Principal Component Analysis

FTIR analysis of the functional groups of the TiO_2/GO membranes was preformed using a Thermo Scientific Nicolet iS5 with ATR module. The measurement was conducted using the wave number interval of 400-4000 cm^{-1} with spectral resolution of 2 cm^{-1}. The reported FT-IR spectra's are averages of 10 scans taken for each sample from the Table 1.

Principal component analysis (PCA) was used for exploratory analysis of the obtained FTIR spectra obtained for the TiO_2/GO composite membranes before and after UV irradiation. PCA performs the projection of the original data values into a set of latent variables (principal components, PC) oriented along directions of maximum variation of the values [35]. Thus, every principal component explains various sources for variation of the data (in this case spectral peaks) and the analysis allows to identify the sources as well as the combination of spectral peaks which are most sensitive to the variation.

PCA analysis usually carried out via investigation of graphical representation of scores and loadings. Scores are projection of the individual measurements to the principal component space. Therefore, scores plot gives information about relationship between the measurements, including trends, groups, outliers, etc. The loadings give information about the relationship between the original variable (wavenumber) and the principal component. Hence, the loading plots show the wavenumbers or peaks responsible for the variation captured by a selected principal component.

The spectra have been preprocessed prior to PCA in order to remove baseline shift (mostly caused by scattering effect) with standard normal variate (SNV) transformation [36]. After that the spectral values were mean centered.

2.4.4 Drop Shape Analysis

Drop shape analysis (DSA) of the TiO_2/GO membranes in table 1 was carried out using a Krüss DSA100 with an automated dispensing unit. DSA was conducted using water (3µl) and diiodomethane

(1µl). An average of 5 contact angle measurements for water and diiodomethane were used to calculate the polar- and dispersive components of the surface energy of the membranes using a combination of Good's and Young's equation derived by Owens and Wendt and Fowkes [37, 38]:

$$(\gamma_s^D \gamma_l^D)^{\frac{1}{2}} + (\gamma_s^P \gamma_l^P)^{\frac{1}{2}} = \gamma_l(cos\theta + 1)/2$$

2.4.5 Zeta potential measurements

The zeta potential of pristine GO and TiO_2/GO membranes were measured using an Anton Paar Sur-PASS electrokinetic analyzer using an adjustable gap cell. The measurements were performed using an electrolyte solution with 0.1 M KCl purged with nitrogen. 0.1M NaOH and 0.05M HCl were used to adjust the pH level during measurements.

3. Results and discussion

3.1. DSC & TGA

The thermal reduction of the pristine GO membranes was investigated using DSC and TGA analysis. Figure 1a shows the DSC curve obtained for the thermal reduction of GO. The endothermic peak in the interval 30 - 125 °C can be assigned to desorption of physical adsorbed H_2O trapped in the GO. An exothermic reduction peak is observed in the interval from 130 °C to 225 °C, due to the reduction of functional groups on the GO sheets. The TGA curve obtained for the GO sample (Figure 1a) show that the largest weight loss also is observed in the interval from approx. 130 °C to 225 °C corresponding to removal of functional groups creating a more pristine graphene structure. The weight loss observed up to 130 °C is ascribed to removal of adsorbed water trapped in the GO layered structure. Figure 1b shows the difference in the weight loss observed for pristine GO membranes reduced at 140 °C and 160 °C. The weight loss for GO reduced at 140 °C and 160 °C were 34,15 % and 47,1 % respectively. The in-

creased weight loss observed for the 160 °C sample is suggested to be due to removal of carboxylic acid and hydroxyl groups based on the principal component analysis of IR data section 3.1.

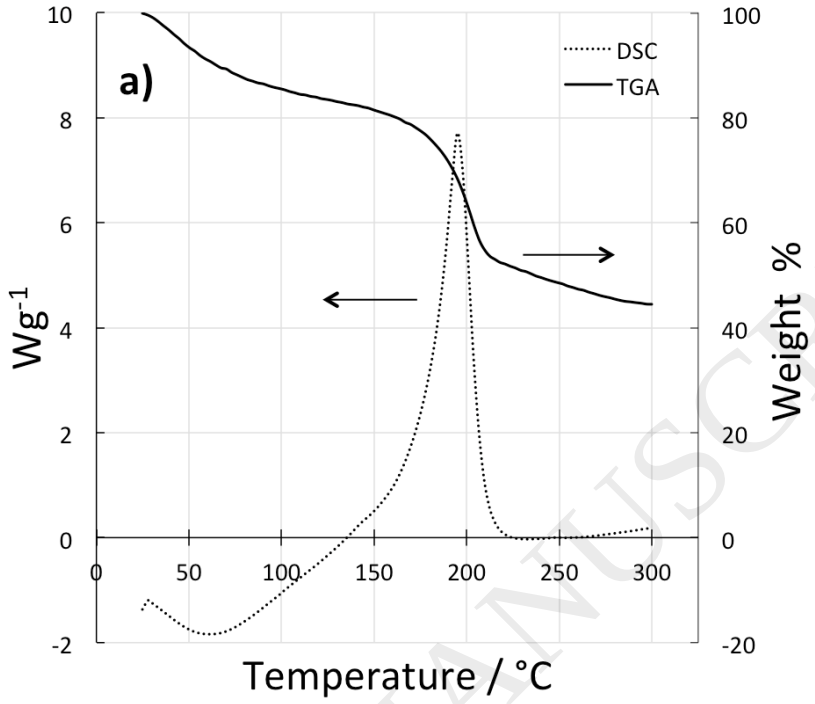

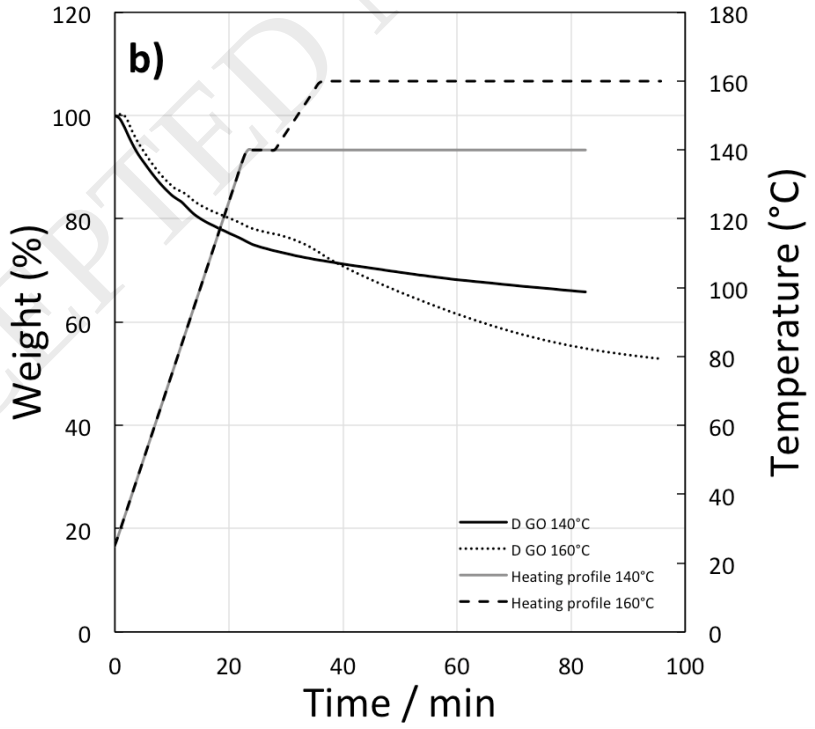

Figure 1. a) Combined DSC and TGA analysis of the GO thermal reduction process (heating rate of 10 °C/min). b) Investigation of weight loss during reduction of GO membranes reduced 1 hour at 140 and 160 °C respectively using TGA.

3.2. XRD

The thermal reduced GO (D) and TiO_2/GO composite membranes (A and C) were examined by XRD to determine the effects of reduction temperature on the GO layer structure of the membranes. The XRD diffractogram of pure GO (D) and TiO_2/GO membranes (A and C) reduced at 140 and 160 °C are shown in figure 2a.

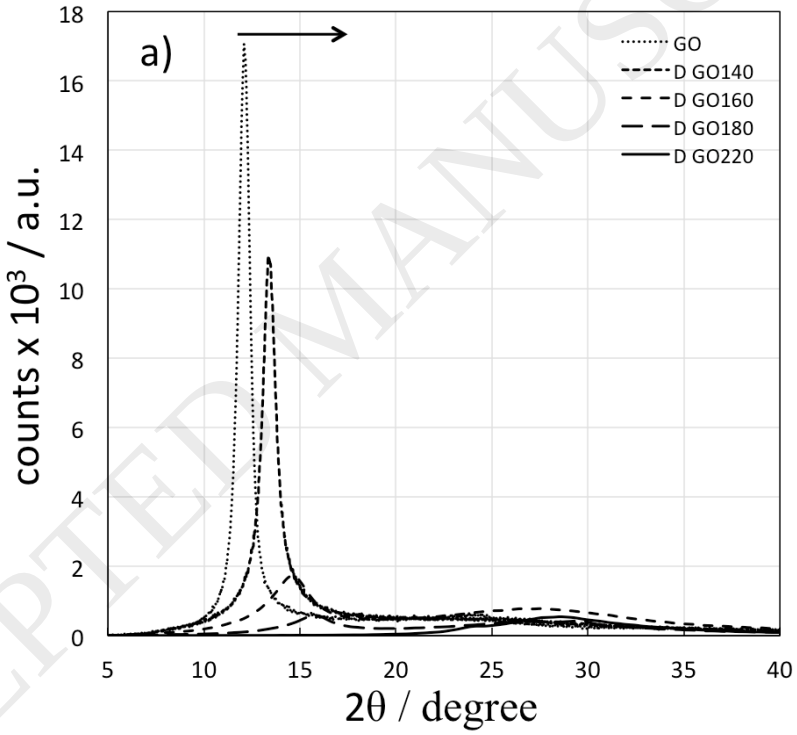

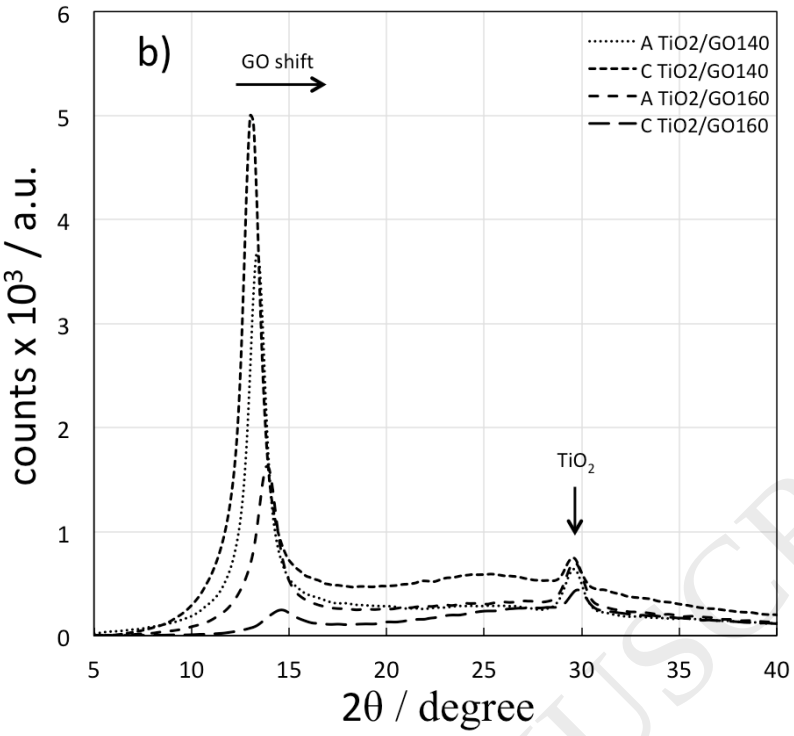

Figure 2. a) XRD diffractogram of pure GO membranes (D) reduced at temperatures 140-220 °C. b) XRD diffractogram of TiO_2/GO membranes with different TiO_2 content (A and C) reduced at 140 and 160 °C.

The peak intensity is significantly higher for the unreduced membrane (GO) compared to GO membranes reduced at 140 and 160 °C (D GO140 and D GO160). Furthermore the peaks shift towards higher angles (2Θ) in the XRD diffractogram. This shift is caused by changes in the structure of the GO membrane due to removal of absorbed/adsorbed H_2O, hydroxyl groups and other functional groups on the GO surface resulting in a collapse of the structure producing a new less ordered structure. The removal of hydroxyl groups and trapped H_2O between the GO layers was confirmed by the TGA curve figure 1b, which shows a significant weight loss for the sample in the reduction temperature interval 130-225 °C.

From figure 3 and table 2 it is evident that the distance between layers (d spacing) in the GO membranes decreases with higher reduction temperature. The significant change in d spacing between 130-220 °C corresponds very well with the observed weight loss interval in the TGA analysis. Furthermore, the

thickness of the layers (D) decreases resulting in a lower number of crystalline layers (N). The formation of a more disordered structure is also apparent from the FWHM; as the crystallinity and homogeneity of the membranes decreases when FWHM broadens. The addition of TiO_2 is not found to change the layers GO structure significantly and the differences observed are more likely caused by a difference in the functional groups on the GO sheets (Figure 3b). The particle size of the TiO_2 nanoparticles used in this investigation is approx. 200 nm in size and thus only changes the membrane structure on a larger scale.

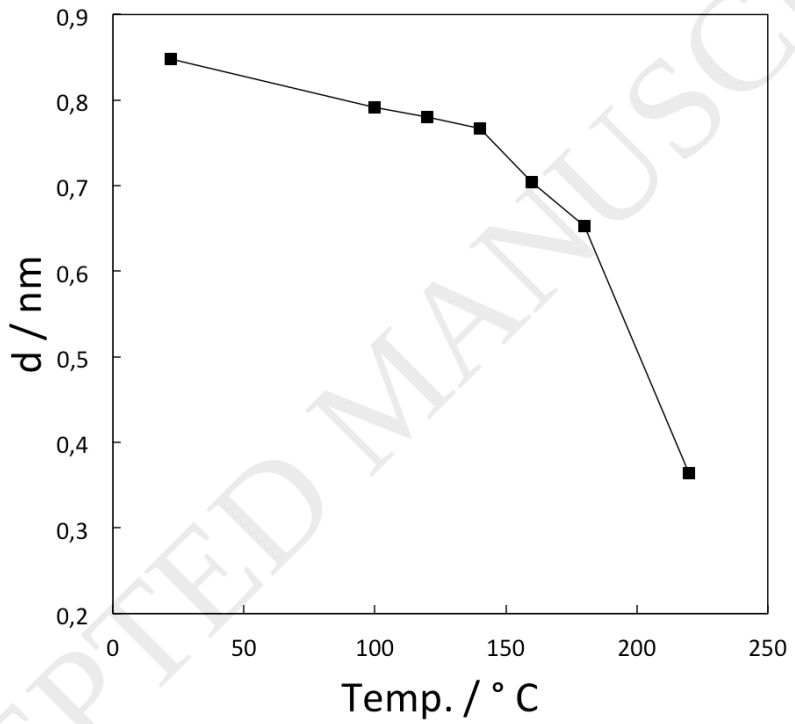

Figure 3. Change in d spacing between the GO layers in pure GO membranes as a function of reduction temperature.

Table 2. XRD peak data and calculated distance between layers (d), thickness of layers D, and estimated number of layers N.

	FWHM	**Peak**	**d** nm	**D** nm	**N**
GO	0.7397	12.106	0.848	12.54	14-15
D GO140	0.9045	13.397	0.767	10.27	13-14
D GO160	2.1091	14.590	0.704	4.41	6-7
D GO180	2.1545	15.758	0.653	4.32	6-7
D GO220	8.3444	28.446	0.364	1.14	3-4
A TiO_2/GO 140	1.0143	13.378	0.768	9.48	12-13

C TiO_2/GO 140	1.1081	13.071	0.786	8.38	10-11
A TiO_2/GO 160	1.4144	13.878	0.741	7.36	9-10
C TiO_2/GO 160	1.5173	14.561	0.706	6.13	8-9

3.3. FTIR

The FTIR spectra of the membranes from Table 1 are shown in Figure 4. The plots on top are original spectra and plots bottom show the spectra after SNV correction. Color groups correspond to the TiO_2 content (from A to D, similar to what is used in Table 1). Apparently, there original spectra have a clear baseline shift due to the scattering effect, which complicates the direct comparison. The shift is removed after SNV preprocessing which allows to reveal several interesting patterns.

The spectra clearly shows most of the peaks characteristic for graphene oxide, including C=O (carbonyl/carboxy) at 1725 cm^{-1}, C=C (aromatics) at 1618 cm^{-1}, C-O (epoxy) at 1225 cm^{-1} and C-O (alkoxy) at 1043 cm^{-1}. There is also a broad O-H peak at 3360 cm^{-1}, which is overlapping with the O-H peak from TiO_2 at 3460 cm^{-1}. The peaks are shown with vertical dashed lines for the plots with preprocessed spectra. Most of the characteristic peaks for TiO_2 are below 1000 cm^{-1} (for example 745 cm^{-1} and 660 cm^{-1}) which is the reason for the high absorption in this region. However, we can still see the effects from these peaks in the region around 880 cm^{-1}, which gives a clear difference for the samples with different TiO_2 content. The area is shown using vertical solid line. The region 2200–2000 cm^{-1} contains strongly absorbing lattice bands for ATR Diamond used in the equipment, which is the most probable reason for the presence of peaks in this region. The small and rather broad peak around 1820 cm^{-1} is associated with carboxylic acids.

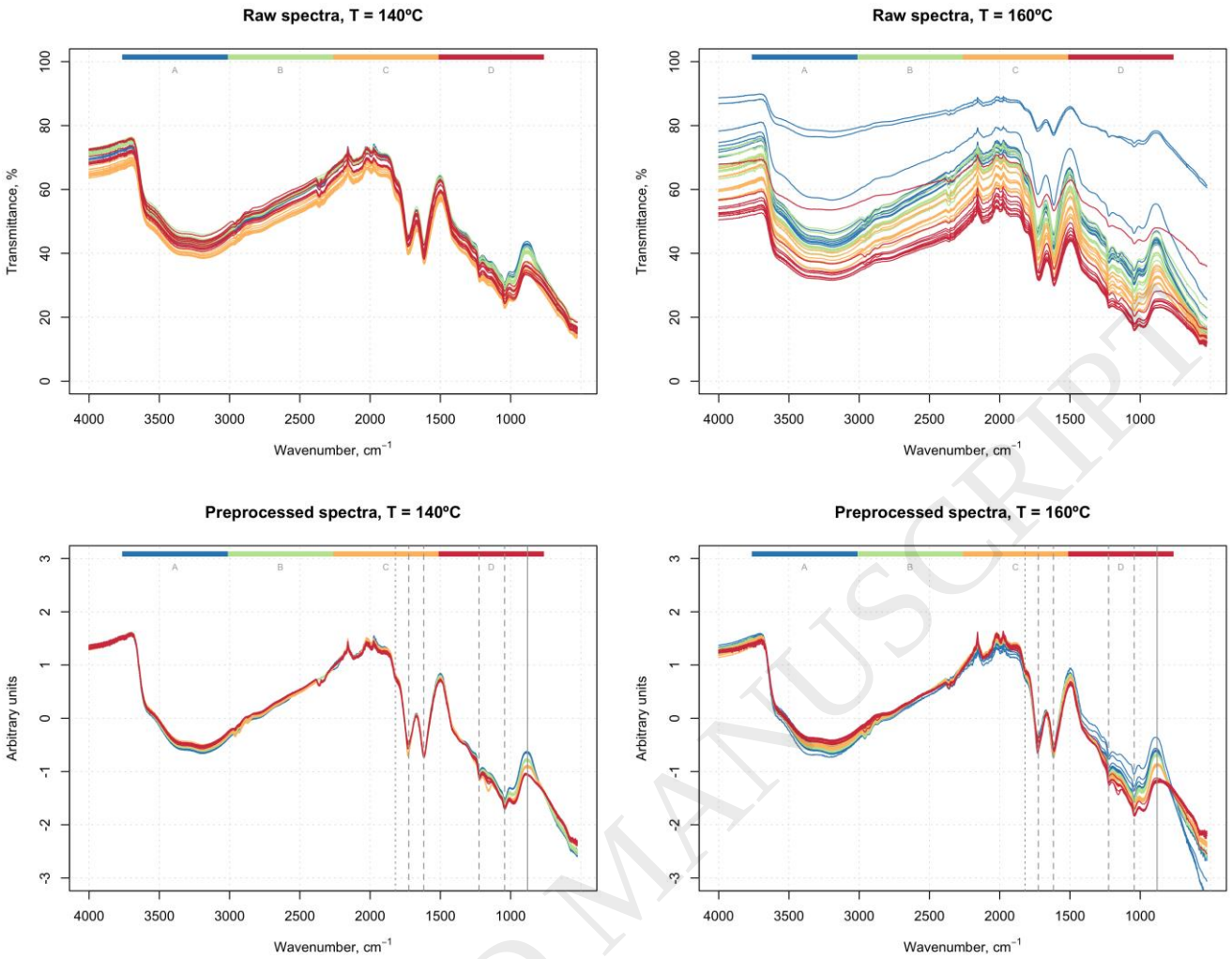

Figure 4. FT-IR spectra of the membranes (top — raw spectra, bottom — spectra after preprocessing). The plots on the left side show spectra for the membranes reduced at 140 °C, plots on the right side show spectra for membranes reduced at 160 °C. The spectra profiles are color grouped according to the TiO_2 content.

Principal component analysis of TiO_2/GO FTIR spectral data

The investigation of spectral variation under several influencing factors can be carried out more efficiently by using principal component analysis. In this a case PCA model was built for the spectra with different TiO_2 content levels (A, B and C), different reduction temperature (140 and 160 ºC) obtained before and after UV activation. Figure 5 shows scores plots for PC1 vs PC2 (left) as well as PC1 vs PC3 (right). The points on the top plots are color grouped by the UV exposure status (before and after) and points on the bottom plots are colored according to the TiO_2 content (A, B and C). The effect of reduc-

tion temperature is visualized by using open circles (T = 140 ºC) and full circles (T = 160 ºC) as marker symbols.

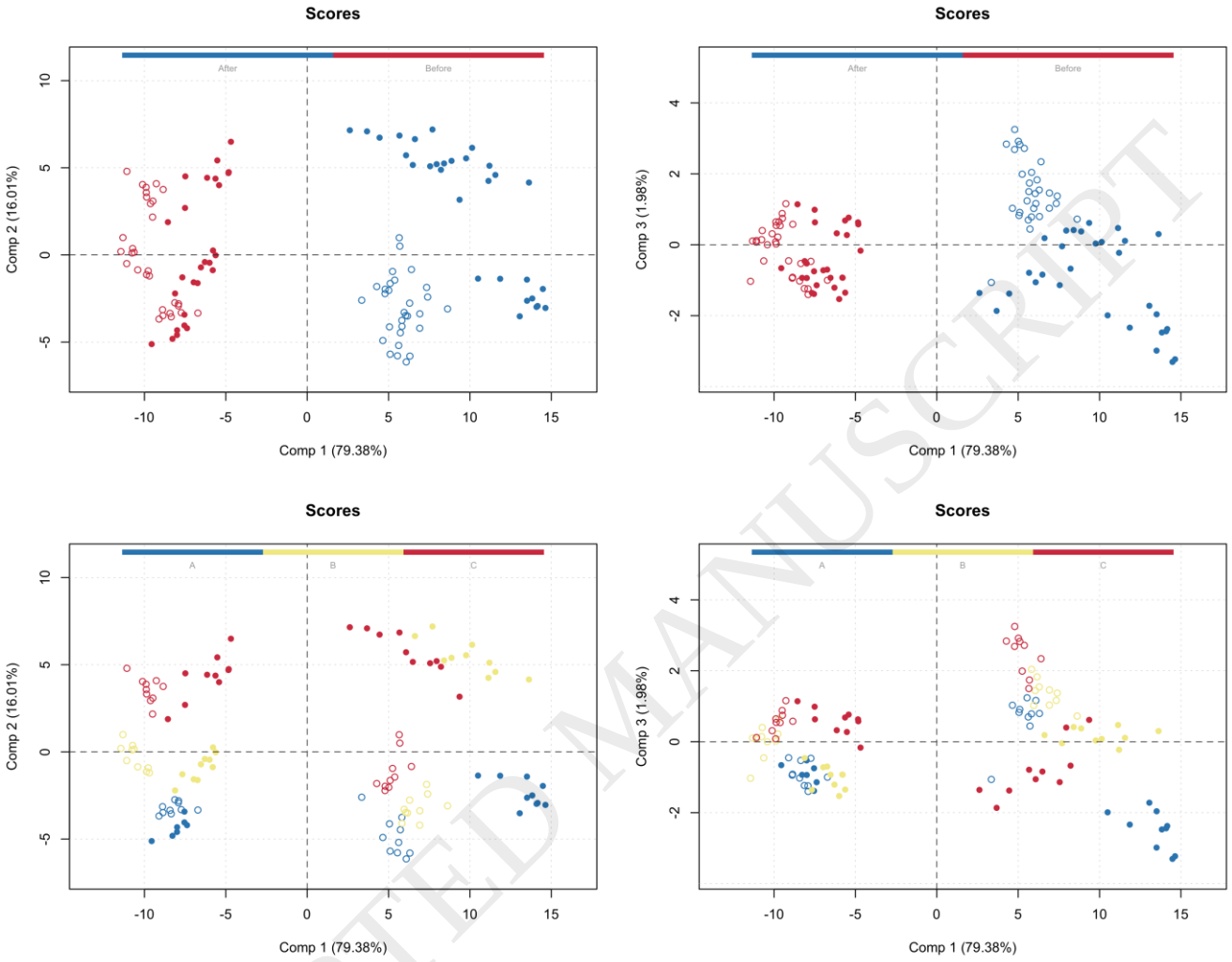

Figure 5. Scores plot for PCA model calibrated using the FTIR spectra acquired for the samples with different TiO_2 content before and after UV exposure. The points are colored by the exposure status (top) and the TiO_2 content (bottom). Open circles show data points for reduction temperature T = 140 ºC and full circles for T = 160 ºC.

Obviously the first principal component explains mostly the variation of the spectral profiles caused by the UV exposure (79.4% of total variance of the data). The second principal component (captures 16% of total variance) is mostly associated with TiO_2 content, especially for the non-exposed samples. The samples after exposure do not show such a clear difference between the B and C TiO_2 levels. PC3 do not show any systematic variation.

The effect from temperature has no systematic pattern but shows different patterns for the samples before and after UV exposure. The score plots for PC1 vs PC2 figure 5 shows that the points for T = 160 ºC are moving to the right for non-exposed samples and to the right and up for the exposed samples. This means that temperature has a different influence for these two groups which is difficult to resolve by the full model.

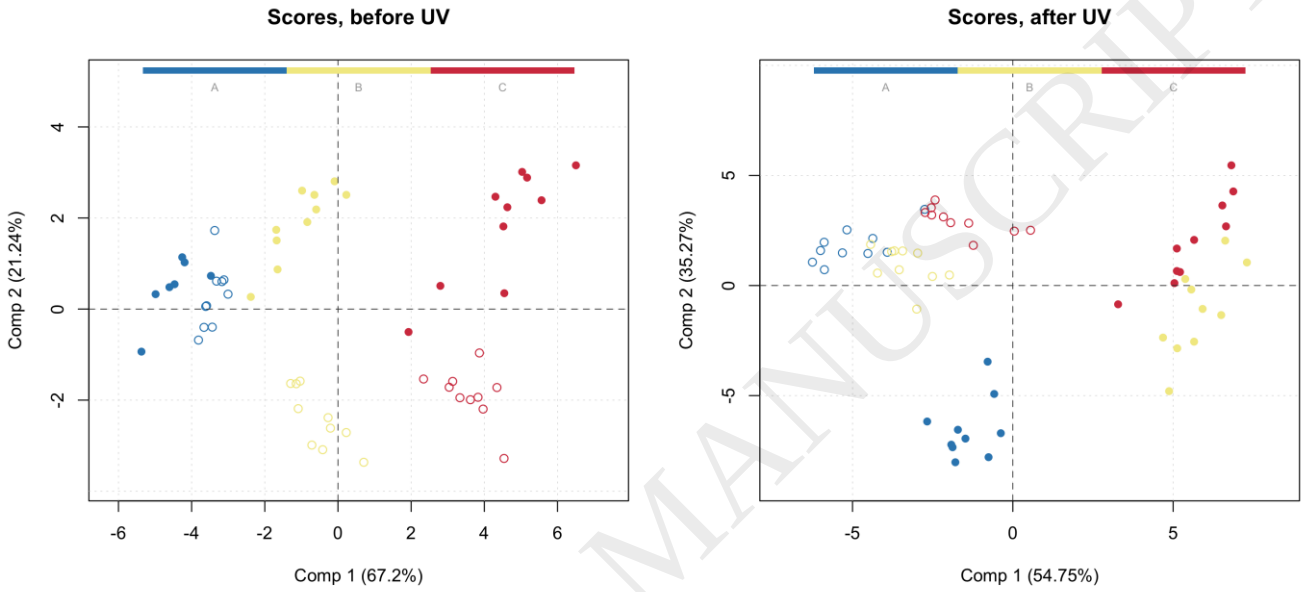

Figure 6. Scores plot for two local PCA model calibrated using only spectra acquired before UV (left) and after UV (right) exposure. The points are colored by the TiO_2 content (bottom), the open circles show data points for T = 140 ºC, full circles — for T = 160 ºC

In order to reveal better the effect of the temperature, two local PCA model have been calibrated — one for the samples before and one for the samples after UV exposure. Figure 6 show the corresponding scores plots. As we can see, for the non-exposed samples there is a clear difference between the effects of TiO_2 content (PC1) and the reduction temperature (PC2) for samples from groups B and C. Moreover, the corresponding directions of variation are orthogonal which means that the effects are independent. In the case of the UV exposed samples there is a clear difference between the samples corresponding to the two reduction temperatures regardless the concentration of TiO_2.

Based on the PCA models the thermal reduction and UV irradiation show similar effect on the IR spectra (PC1 figure 5) for the thermal reduction before UV irradiation and the larger shift observed after UV irradiation suggesting that the first principal component explain the reduction of the GO by both UV and heat treatment. The photoinduced reduction identified by the PCA model is in line with previous reports stating the photoreduction of GO in the presence of TiO_2 [31, 32].

Figure 7 shows loading plots for the first two principal components of the full model (figure 5) in form of line plot. Dashed lines correspond to the location of the peaks similar to the plots shown in Figure 4. As one can see the part of the spectra around 1820 cm^{-1} (carboxylic acid groups) indeed has the highest loading value for the PC1, which is responsible for UV and heating effects. It has been reported that the first groups to be thermally reduced are -OH and -COOH leaving more thermally stable functional group such as ketone on the surface of the GO membranes [39]. In this case only a clear difference is seen for the -COOH group on the loading plot. Two opposing effects cancel out any major changes in the concentration of OH groups present on the TiO_2/GO membrane. I: The electrons generated by activation of the TiO_2 reduce OH functional groups on the GO sheets. II: The photo generated h+ react with adsorbed water to produce OH groups on the surface of the TiO_2 particles. Examination of the IR spectra for the B and C composite membranes reduced at 140 and 160 ºC before UV irradiation show a decrease in the OH groups, which is in line with the TGA analysis.

Another important part is a region around 880 cm^{-1} which was found to be related to the TiO_2 content. As we can see from the scores plot UV exposure changes the spectral response from TiO_2, and this is one of the reasons for the importance of this region for PC1.

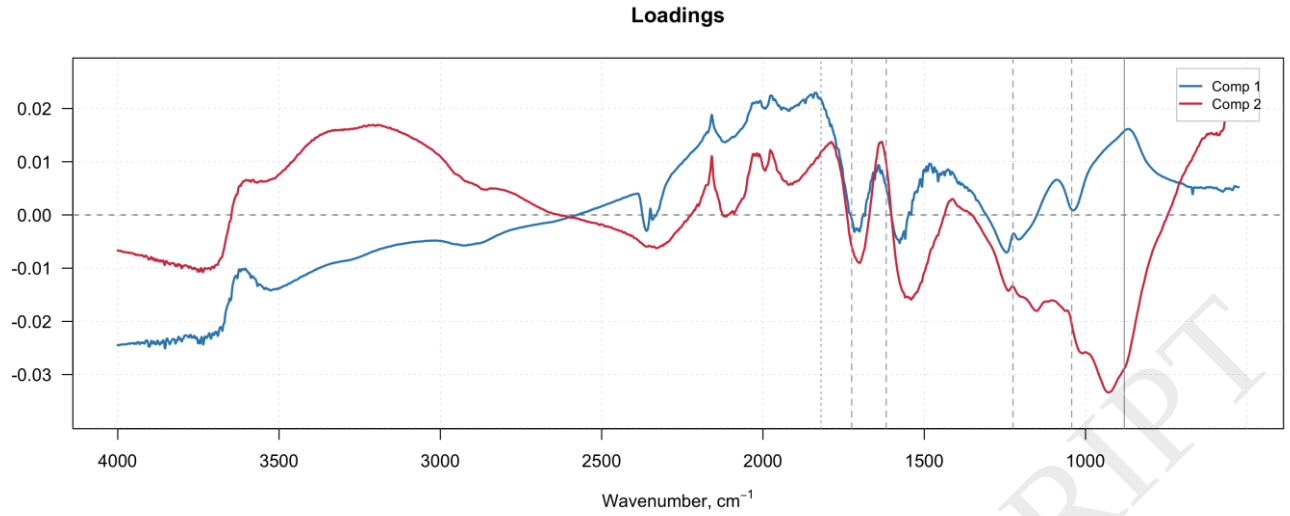

Figure 7. Loading plots for the PCA model.

Loadings for PC2 show a clear influence of similar area around 880 cm^{-1} as well as the broad -OH peak between 3000 and 3600 cm^{-1}, which correspond to the observations from the spectral profiles reported in the previous subsection.

3.4. DSA

The full factorial design in table 1 was used to investigate the influence of TiO_2 content, reduction temperature and UV activation on the surface energy of the TiO_2/GO composite membranes. The results of the drop shape analysis of the TiO_2/GO membranes are shown in (Table 3). Analysis of variance (ANOVA) show the surface energy decreases significantly (α=5) when increasing the reduction temperature from 140 °C to 160 °C. The decrease in hydrophilicity is attributed to a greater loss of carboxylic acid and hydroxyl groups at higher reduction temperatures as observed in the FTIR and TGA analysis. In addition it is found that the surface energy of the TiO_2/GO membranes increases significantly (α=5) with increasing TiO_2 content (A > B > C > D). This is again explained by the higher amount of OH groups present on the TiO_2/GO membranes with increasing TiO_2 content identified by the PCA analysis. The TiO_2/GO composite membranes have lower contact angle (CA) for water resulting in a larger polar

component and higher surface energy than pristine GO membranes. Finally the UV treatment was found to significantly increase the surface energy. The increase in surface energy can be attributed to an increase in the polar component of the surface energy.

The water CA for the TiO_2/GO membranes reduced at 140 °C was found to decrease from 50-65 ° to approx. 20 ° independent on the TiO_2 content after 30 min of UV irradiation. However, the TiO_2/GO membranes with higher TiO_2 contents showed faster hydrophilic conversion rates (Figure 5a). The surface energy of the TiO_2/GO membranes increased from 52-59 mN/m^2 to approx. 73 mN/m^2 corresponding to an average increase of 33 %. No significant change in surface energy was observed for pure GO membranes after UV irradiation (D GO 140 UV).

While all the TiO_2/GO membranes reduced at 140 °C obtained similar hydrophilic state, only the type A membrane (high TiO_2 content) reduced at 160 °C reached a comparable hydrophilic state showing the importance of the TiO_2 in the composite membranes (Figure 8b). This is explained by the PCA model as the UV irradiation for the TiO_2/GO membranes cause a shift to the right and down for the A, B, and C membranes reduced at 140 °C and only the A membrane reduced at 160 °C. Since the vertical motion captures the changes in OH groups only these membrane compositions become highly hydrophilic. In the case of the B and C membrane compositions reduced at 160 °C the UV induced reduction of the GO counteracts the formation of OH groups on TiO_2 resulting in less hydrophilic membranes as explained by the PCA model.

The photoinduced hydrophilic state is suggested to be produced by the temporary formation of hydroxyl groups; already after 10 minutes the membrane has lost much of the hydrophilic properties and after 60 minutes the CA is close to the value before UV irradiation (Figure 8a). In practical applications this switch between the hydrophilic properties could prove to be valuable in order to reduce/hinder membrane fouling.

Table 3. DSA data for water and diiodomethane on pure rGO and TiO_2/GO composite membranes before and after UV irradiation (30 min, 2 mW/cm^2 UVC) (average of 5 measurements). A (high), B (medium), and C (low) TiO_2 content in the TiO_2/GO membranes. Calculated polar and dispersive component, surface energy, and surface polarity. Zeta potential of the membrane surface (Estimated ζ at pH 7 from data in the pH interval 4-9).

	Water	**Diiodomethane**	**P component**	**D component**	**Surface Energy**	**Surface Polarity**	***ζ (pH 7)***
	°	°	mN/m	mN/m	mN/m	%	mW
A TiO_2/GO 140	48.1	27.7	14.8	45.2	59.9	24.7	-24.5
B TiO_2/GO 140	52.0	31.9	13.4	43.4	56.9	23.6	-35.9
C TiO_2/GO 140	65.3	25.6	6.1	45.9	52.0	11.7	-40.0
D GO 140	62.5	36.6	8.8	41.3	50.1	17.6	-26.4
A TiO_2/GO 140 UV	19.8	29	28.1	44.6	72.7	38.4	-35.6
B TiO_2/GO 140 UV	22.0	28.2	28.4	44.9	73.3	39.5	-51.4
C TiO_2/GO 140 UV	21.8	23.9	26.9	46.5	73.4	37.0	-47.5
D GO 140 UV	62.9	33.6	8.1	42.7	50.8	16.0	-
A TiO_2/GO 160	78.9	28.9	1.8	44.7	46.5	3.8	-40.5
B TiO_2/GO 160	80.8	29.1	1.4	44.6	45.9	2.9	-32.8
C TiO_2/GO 160	86.7	29.1	0.4	44.6	45.0	0.9	-42.8
D GO 160	88.8	37.2	0.4	41.0	41.4	0.9	-35.3
A TiO_2/GO 160 UV	20.8	28.9	28.1	44.7	72.7	38.6	-58.5
B TiO_2/GO 160 UV	36.3	29.1	21.3	44.6	65.9	32.3	-46.8
C TiO_2/GO 160 UV	42.5	29.1	18.1	44.6	62.7	28.8	-50.3
D GO 160 UV	85.0	34.1	0.8	42.4	43.2	1.8	-

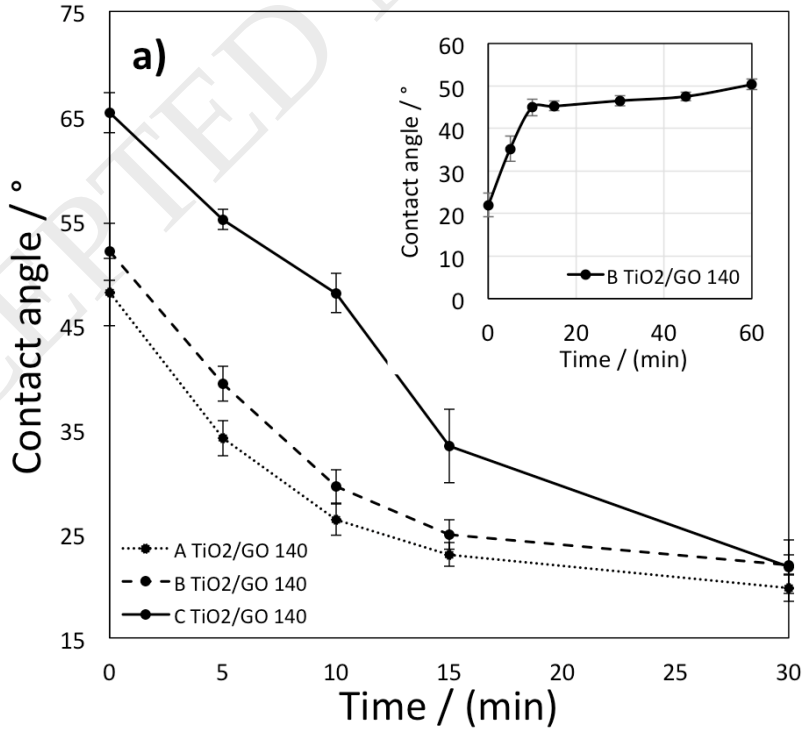

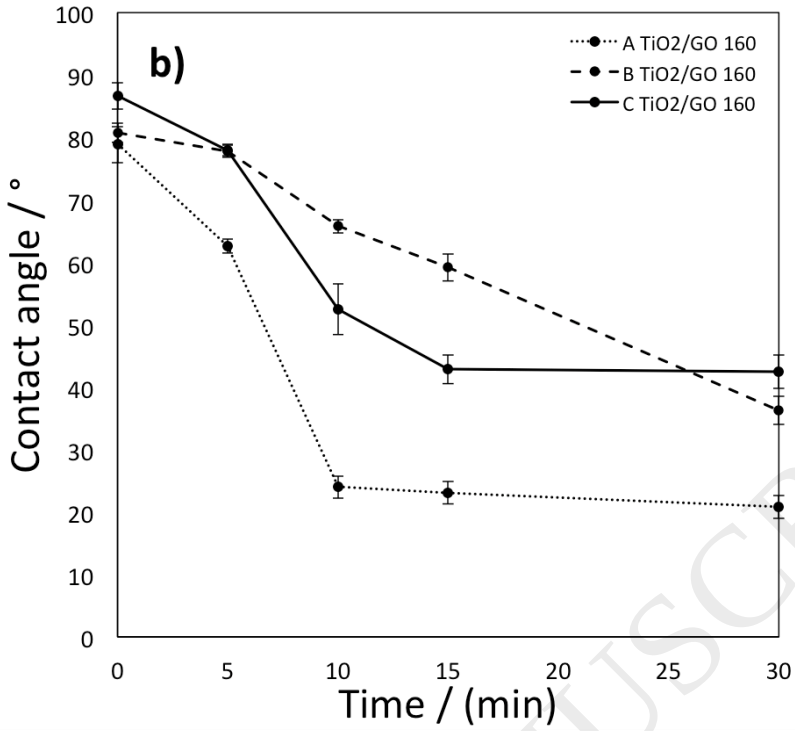

Figure 8. a) Change in water CA as a function of UV irradiation time for TiO_2/GO membranes with different TiO_2 content (A, B, and C) reduced at 140 °C. Insert shows the dark recovery of the initial hydrophobic membrane surface after activation. b) Change in water CA as a function of UV irradiation time for TiO_2/GO membranes reduced at 160 °C. Average of 5 measurements with plotted with standard deviation.

3.5. Zeta potential measurements

The zeta potential for the TiO_2/GO composite membranes in the pH interval 4.5-10 is shown in figure 9. The results show that the Zeta potential of the individual TiO_2/GO membranes are almost constant in the pH interval 4.5-10 (Figure 9). The Zeta potential was not found to vary systematic with the TiO_2 content of the TiO_2/GO membranes or the reduction temperature (Table 3). All the TiO_2/GO membranes were found to have negative zeta potentials varying between -26 and -42 mV. The negative zeta potential is most likely caused by deprotonation of carboxylic acid groups and hydroxyl groups present on the surface/edges of the GO sheets and the TiO_2 in the membranes. A higher TiO_2 content in the composite membrane may not only result in a larger amount of hydroxyl groups but also changes the overall structure of the membranes. Similar the thermal reduction will cause not only a decrease in the number of carboxylic acid and hydroxyl surface groups but also structural changes in the membrane as a decrease

in the d spacing between the GO layers was observed by XRD. The changes in the d-spacing effect the porosity and pore size and hence influence the flow over and into the membrane surface during the streaming potential measurement changing the surface area involved and hence the Zeta potential [40].

UV activation of the TiO_2/GO membranes was found to significantly change the zeta potential of the membranes. In all the tested TiO_2/GO membranes the UV activation resulted in a decrease in the Zeta potential (Figure 9). The change in Zeta potential was found to be largest for GO membranes containing higher amounts of TiO_2. The shift in zeta potential upon UV irradiation supports the hypothesis that hydroxyl groups are formed during the hydrophilic conversion of the membranes.

No visible damage to the membranes was observed in the tested pH interval suggesting that the membranes will be stable under normal working conditions, however above pH 11 the TiO_2/GO composite membranes were found to be unstable and partly dissolved.

Determination of the zeta potential and hydrophilicity are key parameters in characterization of membranes. The zeta potential of the membrane surface provides information about the possible electrostatic attraction/repulsion dependent on the content of the feed stream. In order to achieve the best anti-fouling properties high positive or negative zeta potential of both the membrane and fouling constituents is optimal. The TiO_2/GO membranes were found to have negative zeta potentials ranging from -26 to -42 mV. Activation of the TiO_2/GO membranes resulted in a significant decrease in zeta potential of approx. -15 - -20 mV for the individual membranes. This decrease in zeta potential of the membrane surface enhances the electrostatic repulsion of negatively charged fouling components. In addition the surface energy changed significantly after activation producing a more hydrophilic surface, which hinders adsorption of hydrophobic components often encountered in feed stream. The change in surface properties after activation of the TiO_2/GO composite membranes is significant and hence could be incorporated in the fabrication of antifouling membranes. In this case UV irradiation cycles (On/Off) in combination

with forward/back flushing may be used in easy cleaning membrane systems, where the change in surface properties promote removal of the foulants.

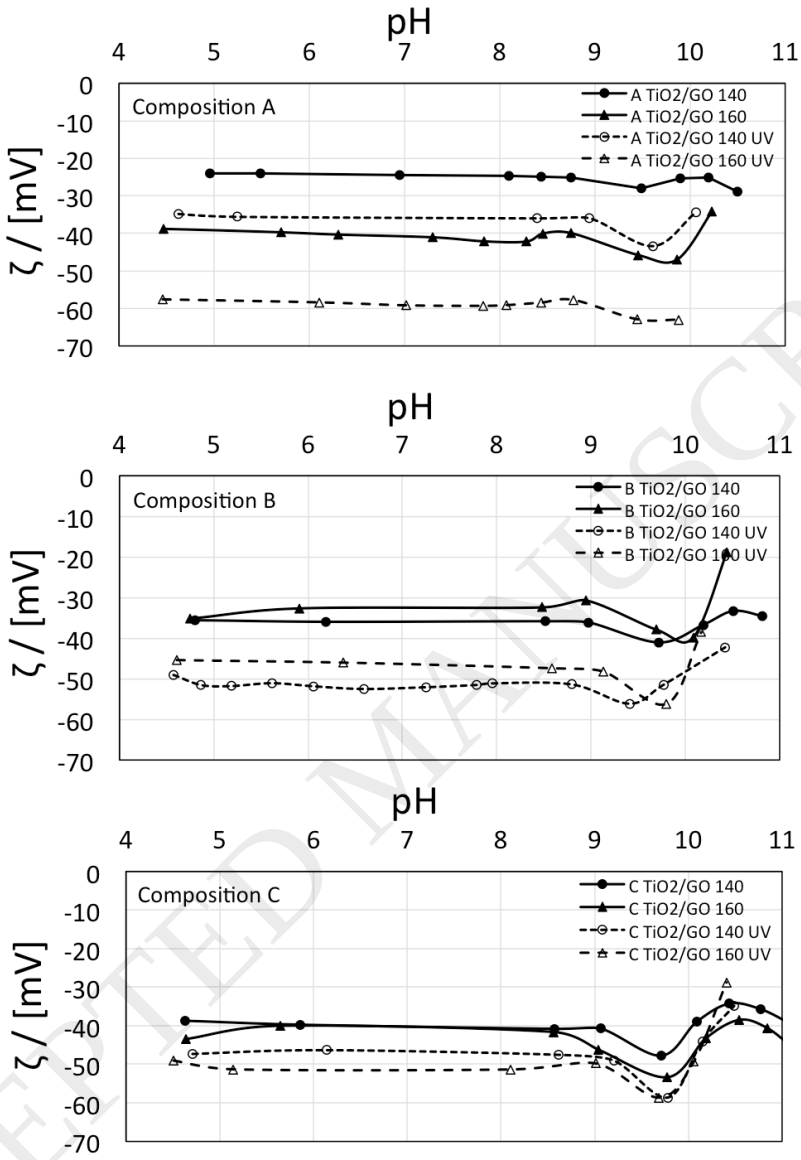

Figure 9. Zeta potential measurements of TiO_2/GO membranes with different TiO_2 content (A, B, and C) reduced at 140 and 160 °C before and after UV activation (30 min, 2 mW/cm^2 UVC).

4. Conclusion

This study concludes that the hydrophilic properties of pure GO (A) and TiO_2/GO composite membranes (A, B, and C) are dependent on reduction temperature; membranes reduced at 140 °C are signifi-

cantly more hydrophilic than membranes reduced at 160 °C. Principal component analysis of FTIR data together with TGA and DSC analysis suggest that the change in hydrophilicity was caused by loss of carboxylic acid and hydroxyl groups when reduced at 160 °C. Moreover XRD analysis showed that the loss of oxygen containing groups results in a less crystalline structure of the membranes.

DSA of the TiO_2/GO composite membranes showed that UV activation increases the surface free energy and hydrophilicity of the membranes. From the PCA model the increase in surface energy is caused by an increase in OH groups on the TiO_2 after activation of the TiO_2/GO membrane. Moreover higher TiO_2 content was found to significantly increase the surface energy of the membranes. TiO_2/GO membranes with higher TiO_2 contents showed faster hydrophilic conversion rates.

In addition UV activation of the TiO_2/GO membranes results in the Zeta potential of the membranes becomes significantly more negative, which will enhance the electrostatic repulsion of negatively charged fouling components. The zeta potential of the individual TiO_2/GO membranes was found to be almost constant in the pH interval 4-9.

References:

1. Y.L. Luo, W.S. Guo, H.H. Ngo, L.D. Nghiem, F.I. Hai, J. Zhang, S. Liang, X.C.C. Wang, A review on the occurrence of micropollutants in the aquatic environment and their fate and removal during wastewater treatment, Sci. Tot. Environ. 473 (2014) 619-641.
2. M. A. Shannon, P. W. Bohn, M. Elimelech, J. G. Georgiadis, B.J. Mariñas, A. M. Mayes, , Science and technology for water purification in the coming decades, Nature 452 (2008) 301-310.
3. F.X. Kong, H.W. Yang, X.M. Wang, Y.F. Xie, Assessment of the hindered transport model in predicting the rejection of trace organic compounds by nanofiltration, J. Mem. Sci., 498 (2016) 57–66.

4. Z. Yan-jun, W. Kai-fen, W. Zheng-jun, Z. Liang, L. Shu-shen, Fouling and cleaning of membranes – a literature review, J. Environ. Sci. 12, 2 (2000) 241-251.
5. L. Ingemar, Surface physics and biological phenomena. Phys. Scr. T4 (1983) 5–13.
6. R. Singh, Membrane Technology and Engineering for Water Purification, second edition, Elsevier, 2014
7. M. Kumar, M. Ulbricht, Novel ultrafiltration membranes with adjustable charge density based on sulfonated poly(arylene ether sulfone) block copolymers and their tunable protein separation performance, Polymer 55 (2014) 354–365.
8. K. Xiao, X. Wang, X. Huang, T. D. Waite, X. Wen, Combined effect of membrane and foulant hydrophobicity and surface charge on adsorptive fouling during microfiltration, J. Membr. Sci. 373 (2011) 140–151.
9. M. Hadidi, A. L. Zydney, Fouling behavior of zwitterionic membranes: Impact of electrostatic and hydrophobic interactions, J. Membr. Sci. 452 (2014) 97–103.
10. D. Breite, M. Went, A. Prager, A. Schulze, Tailoring Membrane Surface Charges: A Novel Study on Electrostatic Interactions during Membrane Fouling, Polymers 7 (2015) 2017–2030.
11. D. Breite, M. Went, A. Prager, A. Schulze, The critical zeta potential of polymer membranes: how electrolytes impact membrane fouling, RSC Adv. 6 (2016) 98180
12. R. K. Josh, S Alwarappan, M. Yoshimura, V. Sahajwalla, Y. Nishina, Graphene oxide: the new membrane material, Appl. Mater. Today 1 (2015) 1-12.
13. H. Huang, Y. Ying, X. Peng, Graphene oxide nanosheet: an emerging star material for novel separation membranes, J. Mater. Chem. A. 2 (2014) 13772-13782.
14. P. Kumar, S. Mural, S. Jain, S. Kumar, G. Madras, S. Bose, Unimpeded permeation of water through biocidal graphene oxide sheets anchored on to 3D porous polyolefinic membranes, Nanoscale 8 (2016) 8048-8057.

15. C. A. Amadei, A. Montessori, J. P. Kadow, S. Succi, C. D. Vecitis, Role of oxygen functionalities in graphene oxide architectural laminate subnanometer spacing and water transport, Environ. Sci. Tech. 51 (2017) 4280–4288.
16. H. B, Park, J. Kamcev, L. M. Robeson, M. Elimelech, B. D. Freeman, Maximizing the right stuff: The trade-off between membrane permeability and selectivity, Science 6343 (2017) 356
17. M. Safarpour, A. Khataee, V. Vatanpour, Preparation of a Novel Polyvinylidene Fluoride (PVDF) Ultrafiltration Membrane Modified with Reduced Graphene Oxide/Titanium Dioxide (TiO_2) Nanocomposite with Enhanced Hydrophilicity and Antifouling Properties, Ind. Eng. Chem. Res. 53, 34 (2014) 13370-13382.
18. Y. Gao, M. Hu, B. Mi, Membrane surface modification with TiO_2–graphene oxide for enhanced photocatalytic performance, J. Mem. Sci. 455 (2014) 349-356.
19. L. M. Pastrana-Martínez, S. Morales-Torres, J. L. Figueiredo, J. L. Fara, A. M. T. Silva, Graphene oxide based ultrafiltration membranes for photocatalytic degradation of organic pollutants in salty water, Water Res 77 (2015) 179-190.
20. G. Rao, Q. Zhang, H. Zhao, J. Chen, Y. Li, Novel titanium dioxide/iron (III) oxide/graphene oxide photocatalytic membrane for enhanced humic acid removal from water, Chem. Eng. J. 302 (2016) 633-640.
21. A. Fujishima, T.N. Rao, D.A. Tryk, Titanium dioxide photocatalysis, J. Photochem. Photobiol. C 1, 1 (2000) 1–21.
22. A. L. Linsebigler, G. Lu, J.T. Yates Jr., Photocatalysis on TiO2 surfaces: Principles, Mechanisms, and Selected results, Chem. Rev. 95 (1995) 735–758.
23. A. Mills, S. Le Hunte, An Overvies of Semiconductor Photocatalysis, J. Photochem. Photobiol. A 108 (1997) 1–35.

24. O. Carp, C.L. Huisman, A. Reller, Photoinduced reactivity of Titanium Dioxide, Prog. Solid State Chem. 32 (2004) 33–177.

25. M.E. Simonsen, Z. Li, E. G. Søgaard, Influence of the OH groups on the photocatalytic activity and photoinduced hydrophilicity of microwave assisted sol–gel TiO_2 film, Appl. Surf. Sci. 255 (2009) 8054–8062

26. M.E. Simonsen, H. Jensen, Z. Li, E.G. Søgaard, Surface properties and photocatalytic activeity of nanocrystalline titania films, J. Photochem. Photobiol. A 200 (2–3) (2008) 192–200.

27. L. Guardia, S. Villar-rodil, J. I. Paredes, R. Rozada, A. Martínez-Alonso, J.M.D. Tascón, Uv light exposure of aqueous grapheme oxide suspensions to promote their direct reduction, formation of grapheme-metal nanoparticle hybrids and dye degradation, Carbon 50 (2012) 1014-1024.

28. T. Wu, S. Liu, H. Li, L. Wang, X. Sun, Production of reduced Graphene Oxide by UV Irradiation, J. Nanosci. Nanotech. 11, (2011) 1-4.

29. B. Xue, Y. Zou, Y. Yang, A UV-light induced photochemical method for grapheme oxide reduction, J. Mater. Sci. 52 (2017) 12742-12750.

30. O. Akhavan, Photocatalytic reduction of graphene oxides hybridized by ZnO nanoparticles in ethanol, Carbon 49 (2011) 11-18.

31. T. Szabó, Á. Veres, E. Cho, J. Khim, N. Varga, I. Dékány, Photocatalyst separation form aqueous dispesion using grapheme oxide/TiO2 nanoparticles, Col. Surf. A: Physicochem. Eng. Aspects. 433 (2013) 230-239.

32. G. Willams, B. Serger, P. V. Kamat, TiO2-graphene nanocomposites UV-assisted photocatalytic reduction of grapheme oxide, ACS Nano 2 (2018) 1487-91.

33. D. C. Marcano, D. V. Kosynkin, J. M. Berlin, A. Sinitskii, Z. Sun, A. Slesarev, L. B. Alemany, W. Lu, J. M. Tour, "Improved synthesis of graphene oxide," ACS Nano 4, 8, (2010) 4806-4814.

34. L. Stobinski, B. Lesiak, A. Malolepszy, M. Mazurkiewics, B. Mierzwa, J. Zemek, P. Jiricek., I. Bieloshapka, Graphene oxide and reduced graphene oxide studied by XRD, TEM and electron spectroscopy methods, j. Elec. Spec. Rel. Phenom. 195 (2014) 145-154.
35. K. H. Esbensen, P. Geladi, Principal Component Analysis: Concept, Geometrical Interpretation, Mathematical Background, Algorithms, History, Practice, Editor(s): Steven D. Brown, Romá Tauler, Beata Walczak, Comprehensive Chemometrics, Elsevier (2009) 211-226.
36. Å. Rinnan, F. van den Berg, S. B. Engelsen, Review of the most common pre-processing techniques for near-infrared spectra, TrAC Trends in Analytical Chemistry, 28, 10 (2009) 1201-1222.
37. D. K. Owens, R. C. Wendt, Estimation of the surface free energy of polymers, J. Appl. Polymer Sci.13 (1969) 1741-1747.
38. F. M. Fowkes, Attractive forces at interfaces, Ind. Eng. Chem. 56, 12 (1964) 40-52.
39. R. Rasuli, Z. Mokarian, R. Karimi, H. Shabanzadeh, Y. Abedini, Wettability modification of graphene oxide by removal of carboxyl functional groups using non-thermal effects of micro-wave, Thin Solid Films 589 (2015) 364-368.
40. T. Luxbacher, The Zeta Guide: Principles of the streaming potential technique, first edition, Anton Paar, Austria, 2014.